


Measurement and Theory of Resonance Raman Optical Activity for Gases, Liquids, and Aggregates. What It Tells about Molecules

Grzegorz Zajac* and Petr Bour*^{*}

 Cite This: *J. Phys. Chem. B* 2022, 126, 355–367

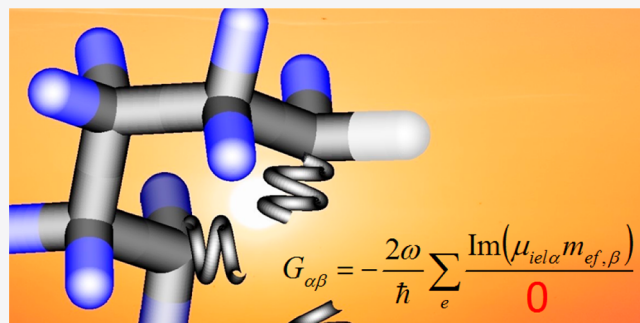
 Read Online

ACCESS |

 Metrics & More

 Article Recommendations

ABSTRACT: Resonance Raman Optical Activity (RROA) appeared as a natural extension of the nonresonance branch. It combines the structural sensitivity of chiroptical spectroscopy with the signal enhancement coming from the resonance of molecular electronic transitions with the excitation laser light. However, the idea has been hampered by many technical and theoretical problems that are being clarified only in recent years. We provide the theoretical basis and several examples documenting the problems, achievements, and potential of RROA, in particular in biomolecular studies.



INTRODUCTION

Nothing has been feared more in the early Raman optical activity (ROA) measurements than color samples. They have been avoided as they often produced a plethora of unwanted effects. The samples decomposed in the laser light, exhibited fluorescence, absorbed the desired Raman signal, or produced instrumental artifacts.^{1,2} Yet, there was one substantial advantage: once the signal could be obtained, it was often quite intense. In this case, nevertheless, the theory to interpret and understand the spectra was missing.

The situation seems to have radically changed during the latest years. Resonance ROA (RROA) revealed interesting information about biomolecules³ and their aggregation,⁴ or even provided means to study nonchiral gases.^{5,6} Reliable measurement protocols have been established,^{7,8} and theoretical procedures for a priori simulations were developed.^{9–12}

RROA is appealing because it makes the (classical/non-resonance) ROA technique more sensitive. ROA has been discovered in 1973¹³ as a small difference in scattering of right- and left-circularly polarized light (CPL) caused by molecular chirality. Thus, a method appeared, suitable to study biologically related chiral systems in solutions. There are not many techniques that can do it, and ROA brought about several advantages. Unlike vibrational circular dichroism (VCD),¹⁴ it was more suitable for the “natural” water environment as water Raman signal in the middle IR region ($\sim 0\text{--}3000\text{ cm}^{-1}$) is relatively small and does not interfere with the measurement. Compared to electronic/UV circular dichroism (ECD, UVCD), ROA bands usually corresponding to fundamental vibrational transitions were more numerous and better resolved. And, of course, ROA is sensitive to chirality, and the intrinsic molecular response to the light is fast (of the order of femtoseconds) so

that the resultant spectrum of conformer mixture is equal to a simple sum of individual species. This may not be true for “chirality-blind” NMR, where a fast interconversion of conformers often results in coalescence of spectral lines.

Soon, applications of ROA followed, including absolute configuration determination for bromochlorofluoromethane¹⁵ or chirally deuterated neopentane.¹⁶ Like all chiroptical methods, ROA is very sensitive not only to the absolute configurations but also to conformation. It was found tremendously useful for studies of saccharides,^{17,18} nucleic acids,^{19,20} peptides,^{21,22} proteins,^{23–25} etc.

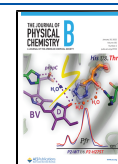
However, vibrational ROA of transparent samples is typically weak in terms of the ROA/Raman intensity ratio (so-called CID,²⁶ circular intensity difference). Typically, CID $\sim 10^{-4}$, which results in the necessity of large amounts ($>1\text{ mg}$) and concentrations ($>20\text{ mg/mL}$) of samples, long measurement times ($\sim\text{hours/days}$), and complicated instrumentation needed for artifact reduction.^{27,28} We estimated that one photon in a million is Raman scattered in a typical experiment; due to the noise in photon detection, we need to record $\sim 10^{10}$ such events to detect ROA spectrum of a reasonable quality.⁸

“Color” samples absorbing the excitation laser light can be achieved by two ways, by making the sample absorb at the excitation frequency (note that 532 nm established as default,

Received: September 23, 2021

Revised: November 3, 2021

Published: November 18, 2021



following commercial ROA spectrometer development²⁸) and by setting the laser light to absorption frequencies. The latter method is much more laborious as it involves construction/adaptation of the spectrometer. When the laser light is in the UV region (e.g., $\lambda \sim 200$ nm), all organic compounds start to absorb and UV-ROA²⁹ becomes synonymous for RROA, similar to that for the nonpolarized Raman scattering.^{30,31} Below, we review some theory advancements and experimental experience with RROA, with an outlook to the future, including advantages and possible drawbacks of the technique.

THEORY

Spectral Intensities. To understand why molecule scatters more when the laser light oscillates with an electronic transition, we need to realize that the Raman intensity depends on molecular polarizability. For example, for a backscattering experiment,^{26,32}

$$I_{\text{Raman}} = I_{\text{R}} + I_{\text{L}} \sim 7\alpha_{\alpha\beta}\alpha_{\alpha\beta} + \alpha_{\alpha\alpha}\alpha_{\beta\beta} \quad (1)$$

where the Einstein summation convention is used for the Cartesian components (α, β) , $\alpha_{\alpha\beta} = \frac{2}{\hbar} \sum_e \frac{\omega_{ei}}{\omega_e^2 - \omega^2} \langle i | \mu_{\alpha} | e \rangle \langle e | \mu_{\beta} | f \rangle$ is the transition polarizability, ω is frequency of the light, angular frequency ω_{ei} corresponds to the difference between the ground (initial, i) and excited (e) molecular state, f is the final state, μ is the operator of the electric dipole moment, $I_{\text{L/R}}$ is the intensity of left/right CPL, and \hbar is the reduced Planck constant. For backscattered ROA and scattered circular polarization (SCP = unpolarized light coming in, CPL is detected) modulation, we get

$$I_{\text{ROA}} = I_{\text{R}} - I_{\text{L}} \sim 8(3\alpha_{\alpha\beta}G'_{\beta\alpha} - \alpha_{\alpha\alpha}G'_{\beta\beta} + \varepsilon_{\alpha\beta\gamma}\alpha_{\alpha\epsilon}A_{\beta\gamma\epsilon}) \quad (2)$$

where $\varepsilon_{\alpha\beta\gamma}$ is the antisymmetric tensor, $G'_{\alpha\beta} = -\frac{2}{\hbar} \sum_e \frac{\omega_{ei}}{\omega_e^2 - \omega^2} \langle i | \mu_{\alpha} | e \rangle \langle e | m_{\beta} | f \rangle$ is a magnetic and $A_{\alpha\beta\gamma} = \frac{2}{\hbar} \sum_e \frac{\omega_{ei}}{\omega_e^2 - \omega^2} \langle i | \mu_{\alpha} | e \rangle \langle e | \Theta_{\beta\gamma} | f \rangle$ a quadrupole polarizability, and m and Θ are the magnetic and quadrupole moment operators.

For the nonresonant case, the transition polarizabilities can be obtained from the (ground state) polarizability derivatives and are available in quantum-chemical software.^{33–36} Origin-independent implementations using London atomic orbitals³⁷ and the density functional theory^{38–40} appear to be the most practical methods for the calculation.

It is clear that when $\omega \rightarrow \omega_{ei}$ all polarizabilities, and thus the Raman and ROA intensities, grow. Of course, at the limit of $\omega = \omega_{ei}$ the expressions above become unusable. Standard means to treat this situation involve “preresonance” calculations when the excitation frequency ω is only close, but not equal, to ω_{ei} for some electronic transition $i \rightarrow e$, introducing a damping parameter Γ and making a substitution $\omega_{e0} \rightarrow \omega_{e0} + i\Gamma/2$, or leaving the “sum-overstate” expressions completely and resorting to a time-dependent treatment.^{9,11,12,41} In the damping and time-dependent approaches, the tensors become complex, and more precise simulations are required to consider the vibronic effects in the electronic transition multipole elements.⁴²

In practice, it is probably impossible to clearly distinguish resonance and preresonance; we use the RROA abbreviation for both cases, and it should be also kept in mind that there is not a sharp border between RROA and the “far from resonance” case (Figure 1).

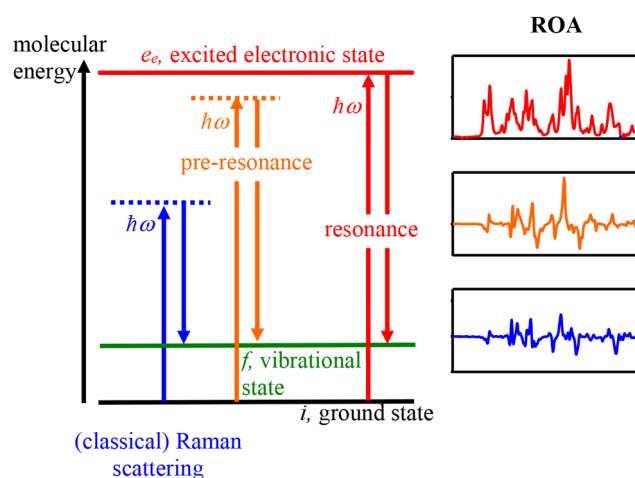


Figure 1. Simplified scheme of ROA experiments. Normally bisignate ROA often becomes stronger in preresonance and monosigned in a resonance; $\hbar\omega$ is the laser excitation energy.

Single Electronic State Limit. A particularly influential in the RROA research was the single electronic state (SES) limit worked out by Nafie.¹⁰ In this case RROA spectrum is just a multiple of the Raman one; i.e., all bands are either positive or negative, dependent on the rotational strength $R = \text{Im}(\langle i_e | \mu_{\alpha} | e_e \rangle \langle e_e | m_{\alpha} | i_e \rangle)$, where the index e marks the involved electronic initial and excited states. The RROA sign is thus dependent on electronic circular dichroism at the excitation frequency, and the CID ratio is proportional to the g (Kuhn’s dissymmetry) factor that can be obtained from a ratio of absorption and ECD spectra. For the backscattered SCP experiment, for example,

$$\text{CID} = \frac{I_{\text{R}} - I_{\text{L}}}{I_{\text{R}} + I_{\text{L}}} = -\frac{g}{2} \quad (3)$$

The single-sign ROA pattern thus quickly became a convenient indicator of the resonance conditions, although, in light of later work, some experiments were attributed to RROA wrongly. It should be said that the Nafie theory, although in most cases probably valid, has been developed for one particular case of a single electronic state and neglects higher-order vibronic effects, such as dependence of the transition multipole moments on vibrational coordinates.^{10,32} Therefore, each experiment should be evaluated individually, and for reliable simulations, more general theories should be preferably used.

Practical Issues. As another RROA advantage, CID increases about 10× compared to the nonresonance case. This is connected to typical vibrational and (about 10× bigger) electronic energies. A less welcome aspect of the SES resonance is the reduction of information that can be obtained about molecular structure (the ROA spectrum is, except for the sign and magnitude, equal to the Raman spectrum). The hope is thus that preresonance experiments or those involving multiple electronic transitions close to the laser excitation provide both benefits, that is enhanced signal and specific RROA spectral features reflecting molecular structure and interactions with the environment.

Although the resonance computations are in general more tedious and less tested than the nonresonance ones and need to be further tested on practical applications, the theory seems to already provide a reasonable basis for further development of RROA. In terms of the quantum-chemical theory level, no special requirements seem to be necessary for RROA modeling,

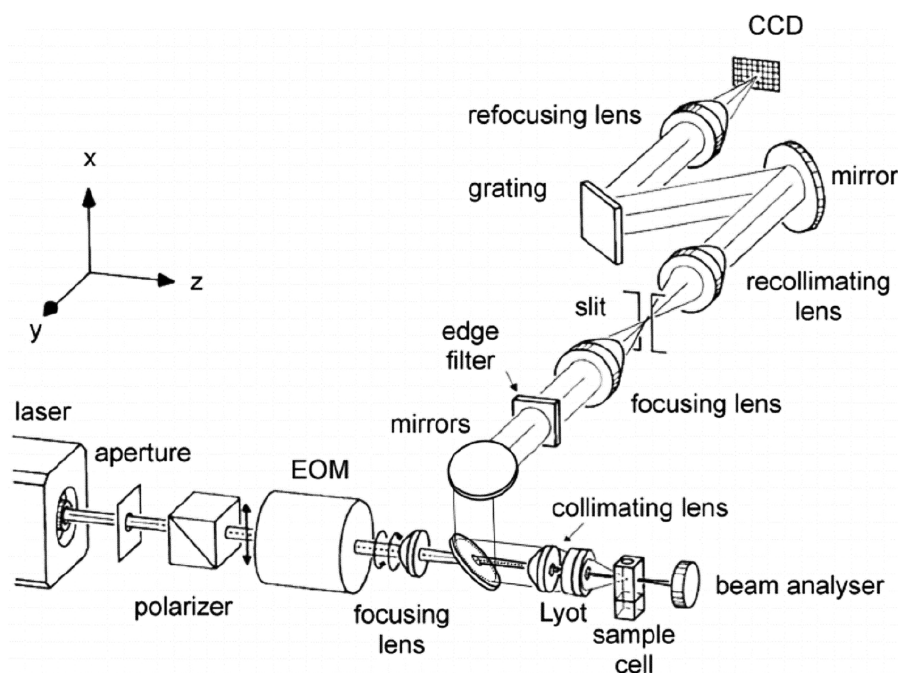


Figure 2. Schematic layout of the DUV ROA spectrometer. Reprinted with permission from ref 29. Copyright 2015 Elsevier.

compared to far from resonance ROA. Thus, hybrid functionals, such as B3LYP, continuum solvent models, and standard medium-sized basis sets, such as 6-31++G**, already provide usable results.^{11,12} For metal complexes, however, a newer functional (M11Plus) was suggested as a better alternative.⁴³

MEASUREMENT

For compounds absorbing light at the laser excitation frequency, RROA and resonance Raman (RR) measurements do not require special adaptation of ROA spectrometers. Nevertheless, special handling is needed for such samples, namely lower concentrations and laser powers to prevent overheating and decomposition. The most common 532 nm laser wavelength is about in the middle of the visible spectrum, and there is a high probability that any colored molecule will exhibit RROA. When the absorption occurs at different wavelengths we need to adapt the instrumentation. Tuning the laser excitation frequency to achieve the resonance in one instrument is difficult and rather rare.³² On dedicated instruments, however, apart from the standard SCP/532 nm setup, RROA was reported with incident or dual circular polarization modulations (ICP = incident CPL, unpolarized light detected, DCP = CPL used both in incident polarization and detection), and 785, 780, 514.5, 488, 457, and 244 nm laser lines. The first RROA experiments were done using the DCP modulation and 514.5 nm.^{2,29,32,44–46}

Using the 780 nm excitation was originally suggested as a mean to reduce fluorescence of trace impurities, problematic for the 532 nm case. In particular, samples from living organisms are often difficult to purify.^{44,47} For the same reason, the 1064 nm excitation was considered, but the ROA experiment appeared problematic.^{29,48} As the Raman/ROA intensities are also inversely proportional to the fourth/fifth power of the wavelength,^{26,49} their recording is quite difficult for longer wavelength, and a resonance is very helpful here. The different (fifth) power for ROA comes from the time-dependent perturbation theory and the need to include higher terms in molecule-light interaction potential. The enhancement under

resonance was used in ICP/785 nm RROA measurements of proteins possessing chromophores absorbing within 400–600 nm.^{45,50,51} The spectra were enhanced but still bisignate, that is providing additional information to plain Raman scattering and ECD. However, due to the $\lambda^{-4}/\lambda^{-5}$ dependencies, also the average CIDs diminish. Compared to the 532 nm line, they were found to be about 1.5 times smaller for 780 nm.⁴⁴

For a shorter wavelength, resonance conditions have been probed for many proteins or nucleic acids during nonpolarized Raman experiments.^{30,31,44,52} It is interesting that also here the fluorescence may be significantly reduced close to the UV region compared to the 532 nm excitation, due to relatively narrow range of the Raman spectra and large Stokes shifts of the unwanted emission bands.^{29,31} An SCP-ROA spectrometer with 457 nm laser has been constructed.⁴⁶ Although construction of ultraviolet ROA spectrometers using even more energetic radiation is quite challenging, an ICP instrument operating at 244 nm has also been presented (Figure 2).²⁹ It can offer the increase of intensity, higher CIDs, lower fluorescence, and smaller sample amounts and laser powers needed. On the other hand, it requires special optics and the samples quickly decompose. Strong absorption of incoming laser light may cause overheating, while absorption of the scattered light also diminishes the signal before it reaches the detector. These problems can be mitigated by lowering the concentrations, focusing the incident radiation close to the front of measurement cell, and rotating or spinning the cells.

INTERFERENCE OF ECD AND RROA

In color, resonating samples circularly polarized light (a nonzero imbalance, $I_R - I_L$) is produced not only by RROA itself but also by electronic circular dichroism.³² The polarization generated by ECD can be further changed due to (“ordinary”) Raman scattering. This effect has been ignored in many RROA studies, but may lead to wrong interpretation of experimental data. The most blatant example is probably “RROA” of achiral solvents, observed in a presence of chiral solutes. This “false ROA” is

caused by solute ECD, when combined with repolarization on solvent molecules during Raman scattering, and is generally always present.⁵³

The ECD-Raman effect has been first wrongly attributed to solvent–solute complexation^{54,55} or explained only partially by a “ring of fire” distant solvent–solute interactions.⁵³ Only lately has the phenomenon been explored in detail using two-cell experiments, and a quantitative formula has been derived enabling to simulate the spectra precisely.⁷ When taking into account usual SCP measurement conditions, we can calculate CID for this CPL imbalance as⁸

$$CID_{ECD-Raman} = \left(1 + \frac{2L'}{L}\right) \frac{\Delta\epsilon' + DOC \Delta\epsilon}{4} cL \ln(10) \quad (4)$$

where L' is optical path not involved in the scattering, L is the Raman-active path length, $\Delta\epsilon$ and $\Delta\epsilon'$ are ECD intensities at the excitation and scattered wavelengths, respectively, c is concentration, and DOC is the degree of circularity.

Note that DOC is unique of each vibrational transition. It can be measured²⁸ or calculated. For backscattering,^{7,26,32}

$$DOC = 5 \frac{\alpha_{\alpha\beta}\alpha_{\alpha\beta} - \alpha_{\alpha\alpha}\alpha_{\beta\beta}}{\alpha_{\alpha\alpha}\alpha_{\beta\beta} + 7\alpha_{\alpha\beta}\alpha_{\alpha\beta}} \quad (5)$$

It is important to realize that DOC has nothing to do with chirality; it just determines how the light polarization is changed during the Raman scattering. For example, if the sample is irradiated by right CPL (and not by unpolarized light as for SCP ROA), DOC is equal to CID ($(I_R - I_L)/(I_R + I_L)$, eq 3).²⁸ Because for 90° scattering DOC is zero, the right angle geometry may be perhaps used to minimize the ECD influence on ROA.^{26,56} This, however, would require building dedicated instruments, and it may result in an overall decrease of the signal intensity.

Separating the ECD-Raman signal from the true vibrational RROA is thus essential for further advances of the RROA spectroscopy, especially when latest experimental and theoretical results suggest that the first contribution is usually much larger.⁴³ The separation based on formula 4 may be combined with a variation of the concentration and focal region.⁸ Nevertheless, also ECD-Raman itself has been shown to be usable in analytical chemistry, as a form of ECD or chirality detection.⁵⁷

The danger stemming from the ECD-Raman and RROA mixing can be documented in Figure 3, where ROA spectra of a vitamin B₁₂ derivative have been measured in two cell positions,

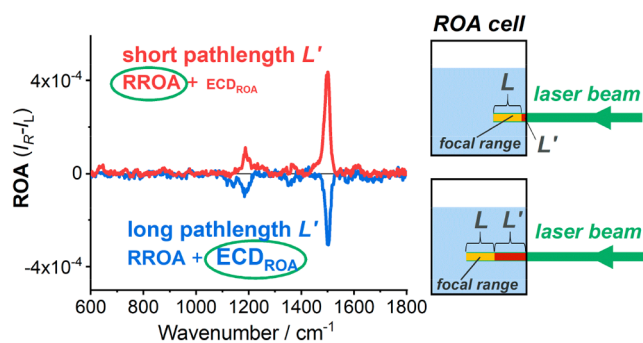


Figure 3. ROA spectra of (CN)13-epi-Cbl(e-lactone) at the 0.8 mg/mL concentration measured for different cell positions. Reprinted with permission from ref 8. Copyright 2021 Wiley.

farther and closer to the incoming laser beam. The position change resulted in a sign change of the recorded spectrum(!). Fortunately, this can be explained on the basis of eq 4, as the ECD-active, but Raman-inactive optical path (L') makes the ECD-Raman component more important.

EXAMPLES OF RROA AND RELATED EXPERIMENTS

Single and Multiple State Resonance. The first experimental observation of the RROA was reported in 1998

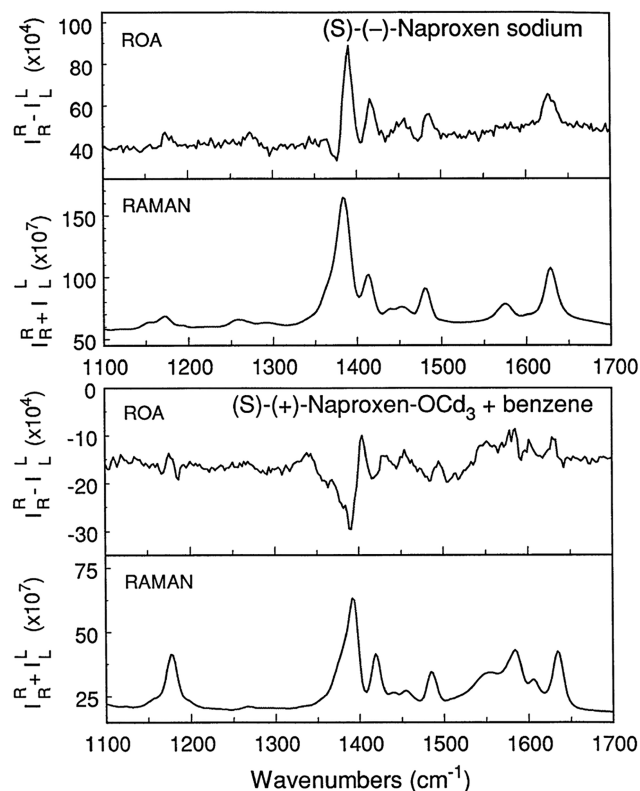


Figure 4. ROA (DCP₁ modulation) and Raman spectra of (S)-(-)-naproxen sodium (top) and (S)-(+)-naproxen-OCd₃ (bottom). Reprinted with permission from ref 2. Copyright 1998 Elsevier.

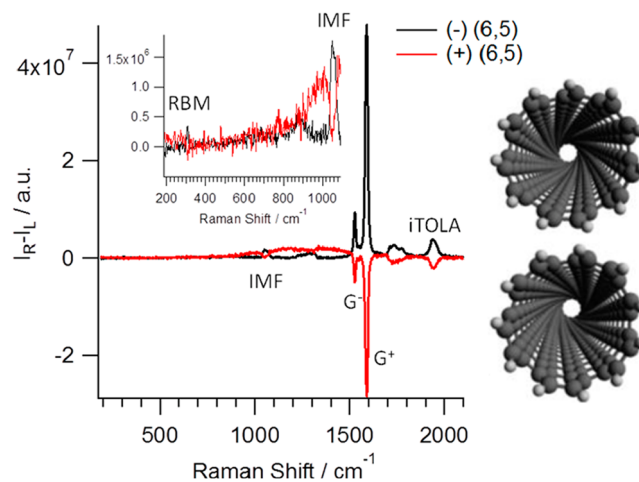


Figure 5. ROA of SWCNT enantiomer suspensions. Reprinted with permission from ref 64. Copyright 2016 ACS.

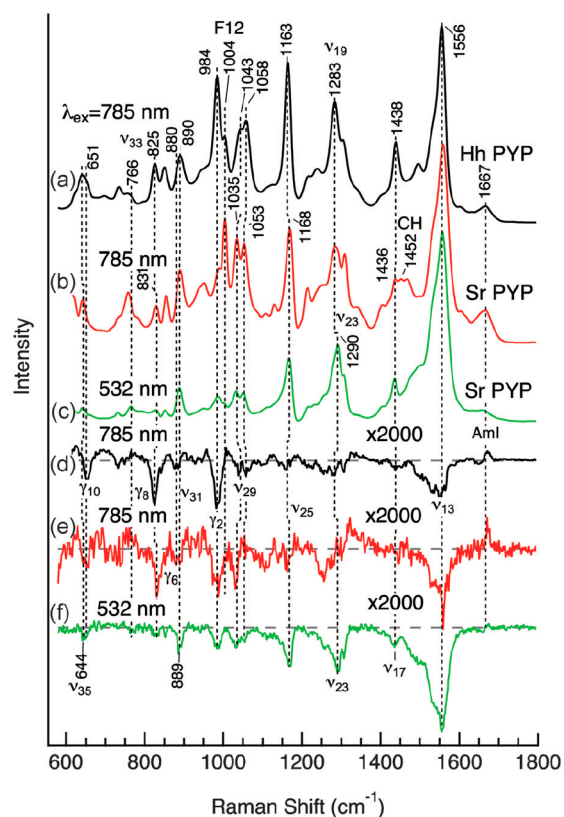


Figure 6. Raman and ROA spectra of a photoactive yellow protein obtained with the 532 and 785 nm excitations. Reprinted with permission from ref 50. Copyright 2015 John Wiley and Sons.

by Varghek et al.² It confirmed the preceding predictions of the SES theory¹⁰ in that the for (*S*)-(-)-naproxen sodium spectrum was mostly positive and about proportional to the Raman signal (Figure 4, top). For the methyl ester of the compound an opposite sign was obtained (Figure 4, bottom). The RROA signs correlated with ECD. However, the CID ratio $\sim 4 \times 10^{-4}$ was not particularly high as it was measured under preresonant conditions, with a large energy difference between the 514 nm excitation line and resonant 330 nm transition. The interpretation of experimental results was later confirmed by quantum-chemical calculations, using both sum-over-states (SOS) and time-dependent expressions.^{58,59}

After almost a decade, two studies appeared, reporting RROA spectra of myoglobin and cytochrome *c*.^{60,61} Here the signal was bisignate, implying that it is related to a resonance with at least two electronic states. A spectrum reported for other natural product, a marine antibiotic, also exhibited RROA features.⁶²

At 2012, RROA spectra of bis(trifluoroacetylcamphorato) copper(II) complex were analyzed on the basis of two electronic states contributing to the signal.⁶³ The SES mechanism was applied independently to the states, and their different contributions to different RROA bands were discussed. The 532 nm laser was used, and the experimental results were verified by measuring both enantiomers. The spectra were rather unusual: RROA bands within 830–1600 cm^{-1} were all negative for the (*R*)-enantiomer, and only one band (C=O stretching at 1640 cm^{-1}) was positive. The negative RROA bands were related to a resonance with electronic transitions within 261 and 315 nm, whereas the positive signal was assigned to a transition at 395 nm.

After exploration of small organic molecules and chiral metal complexes, RROA spectra of single-walled carbon nanotubes (SWCNTs, Figure 5) brought the technique to yet another realm of compounds.⁶⁴ Here the 532 nm laser line was quite close to the 570 nm E_{22}^S electronic transition. Most of the bands were monosignate, especially strong were the G-bands (G^+ at 1589 and G^- at 1526 cm^{-1}). The SES theory appeared valid in this case, the RROA sign was opposite to ECD of the E_{22}^S transition, and the $-g/2$ rule (eq 3) was satisfied. Higher than expected CIDs of some less intense bands were explained by an influence of another excited state, noise, and experimental errors. Quantum-chemical modeling of SWCNTs' RROA followed soon.^{65,66}

Similarly, as for the nanotubes, helicenes also can be thought of as functional carbon materials. In this context, it is interesting that the ROA was applied for two iron alkyl species with redox-triggered chiroptical switching.^{67,68} The 532 nm laser line coincided with electronic absorption, giving enhanced spectra, RROA was monosignate, opposite in sign to the ECD band at 532 nm, and the dissymmetry factor and CID ratios were close to $-g/2$. This interpretation was confirmed by TD-DFT calculations.

Biologically Relevant Systems, Proteins. An actively pursued research direction comprises functional colorful proteins, often containing metal ions, because of the connection to the biology. For a photoactive yellow protein from *Salinibacter ruber*, Haraguchi et al. reported in 2015 resonance ROA in a single experiment (Figure 6).⁵⁰ With the 532 nm excitation most of RROA bands were negative and assigned to the *p*-coumaric acid chromophore, except for a nonresonant protein amide I (C=O stretching) band at 1667 cm^{-1} . With the 785 nm laser, relative intensities of the chromophore bands were smaller, but still enhanced due to the preresonance. The sign was opposite to ECD of the lowest-energy $\pi \rightarrow \pi^*$ electronic transition around 434 nm.

Another example of preresonance ROA of orange carotenoid protein (OCP) was reported in 2017 by Fujisawa et al.⁵¹ The protein is responsible for photoprotection of photosynthetic cyanobacteria. It contains a chiral carotenoid chromophore (3'-hydroxyechinenone) absorbing light within 400–600 nm. ECD is relatively strong as well, due to distortion of the polyene chain induced by the binding to the protein. Moreover, two forms of the protein (OCP^O , OCP^R) provided distinct absorption and ECD signals, and they also gave distinct preresonance ROA. ECD maxima were located quite far, at 475–485 nm from the 785 nm excitation line. The ROA bands were almost all negative and opposite in sign to ECD. However, relative ROA intensities did not follow the Raman spectra, and the CID ratios were approximately three times bigger than predicted by the SES theory. The change of chromophore conformation in OCP^O and OCP^R was reflected in the shift of the in-phase C=C stretching vibration, from 1523 cm^{-1} for OCP^O to 1517 cm^{-1} for OCP^R . Also a hydrogen out of plane mode at 980 cm^{-1} was quite sensitive to it, and the experimental results were rationalized by quantum chemical calculations.⁵¹

Scammato et al. in 2019 reported bisignated RROA of the imidazole–myoglobin complexes as a function of molar excess of the imidazole ligand.⁶⁹ Also here a structural sensitivity of RROA was reported, to conformational changes induced by the concentration variation. The 532 nm laser line was in resonance with electronic transitions (*Q*-bands) of the heme chromophore in myoglobin. It had an absorption maximum at 534 nm, and the whole 400–600 nm range in myoglobin and its imidazole

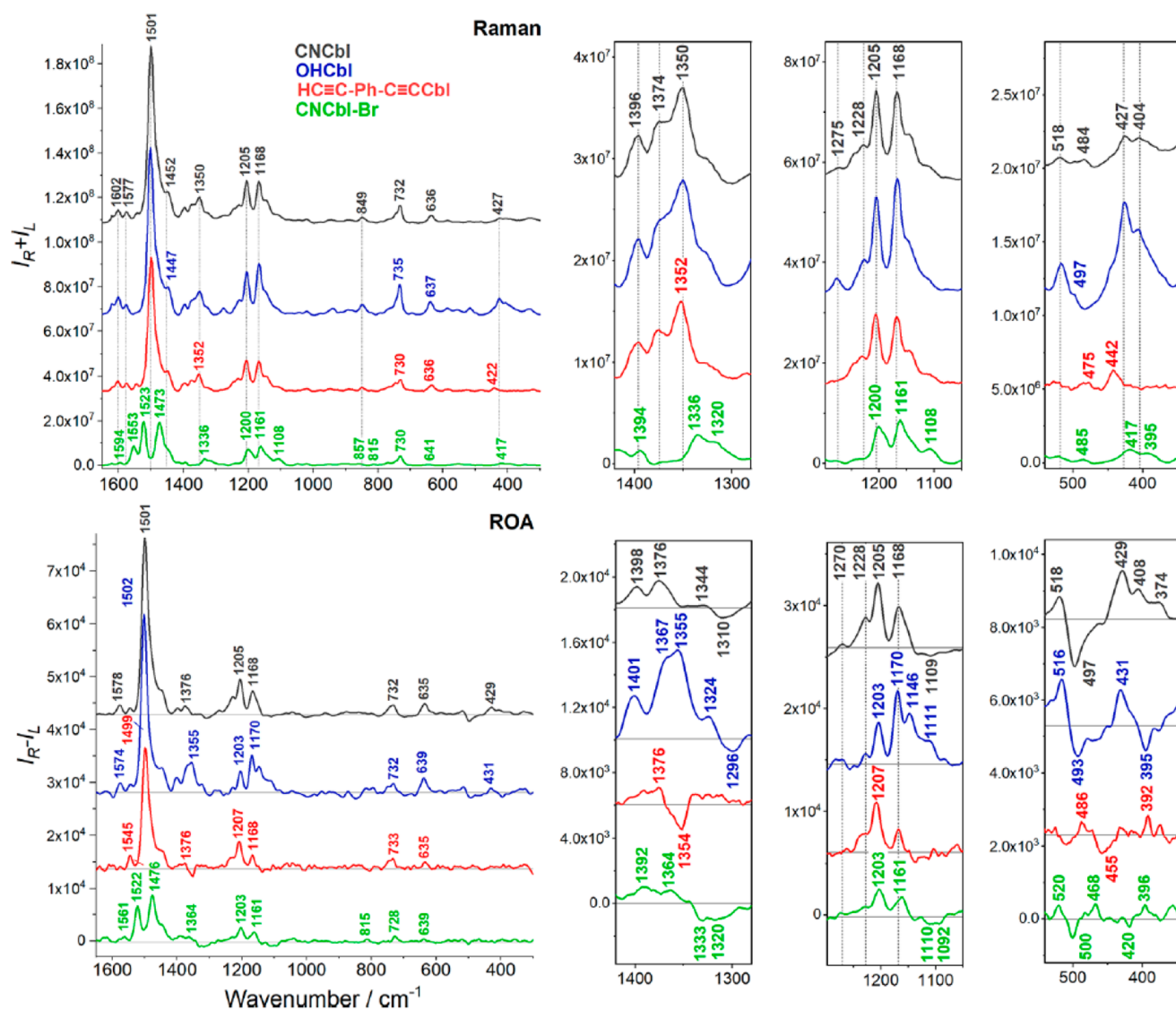


Figure 7. Raman and ROA spectra of cobalamins with different upper axial substituents: black, cyanide; blue, hydroxyl; red, 1,4-diethynylbenzene; green, CNCbl bromine ring derivative. Reprinted with permission from ref 3. Copyright 2020 ACS.

complexes relevant for ROA comprised positive ECD bands. Bisignated RROA bands were therefore related to a splitting and complex interactions of the *Q*-bands. However, because for the main vibrational bands in the imidazole-myoglobin complexes the CID ratios followed the $-g/2$ rule, resonance with a single electronic state was suggested to be the major contributor to RROA intensity.

More recently, Bogaerts et al. have measured complex resonance and nonresonance ROA spectra of a glycoprotein, human serum transferrin (HuTf).⁷⁰ The resonance with the 532 nm excitation was due to the presence of the Fe(III) ion in the holo form of HuTf. Four enhanced ROA bands at 1170, 1284, 1506, and 1608 cm^{-1} were assigned to phenolate vibrations in the Fe(III) binding pocket. The RROA bands were positive, opposite in sign to the resonating ECD bands at ~ 460 nm, and CID ratios were about equal to $-g/2$ at 532 nm. In the monoferric form of HuTf, the RROA intensity was diminished and protein ROA bands were more visible. RROA thus could “sample” the active site of the protein, while information about

the protein secondary structure was still available from nonresonance ROA.

In two papers published in 2020 by Machalska et al., RROA spectra of vitamin B₁₂ derivatives exhibited surprising variability.^{3,71} Cyanocobalamin, CNCbl, and its analogs were measured with the 532 nm excitation (Figure 7). The RROA spectra were mostly positive and opposite in sign to ECD of the lowest-energy electronic bands, corrinoid macrocycle $\pi \rightarrow \pi^*$ transitions within 480–550 nm. Some RROA bands below 600 cm^{-1} of lower intensity but high CIDs were negative; these were assigned to cobalt–upper axial ligand vibrations. The negative sign was probably due to the resonance with a positive ECD band. For CNCbl this band at 433 nm was related to electronic transitions involving cobalt 3d and CN- π molecular orbitals. CID magnitudes mostly did not obey the $-g/2$ relation, but the signs did, and the experimental results were reasonably well reproduced by DFT preresonance ROA calculations using the Gaussian software.³

Aggregation-Induced RROA (AIRROA). During aggregation, electronic transitions of molecules can change and become

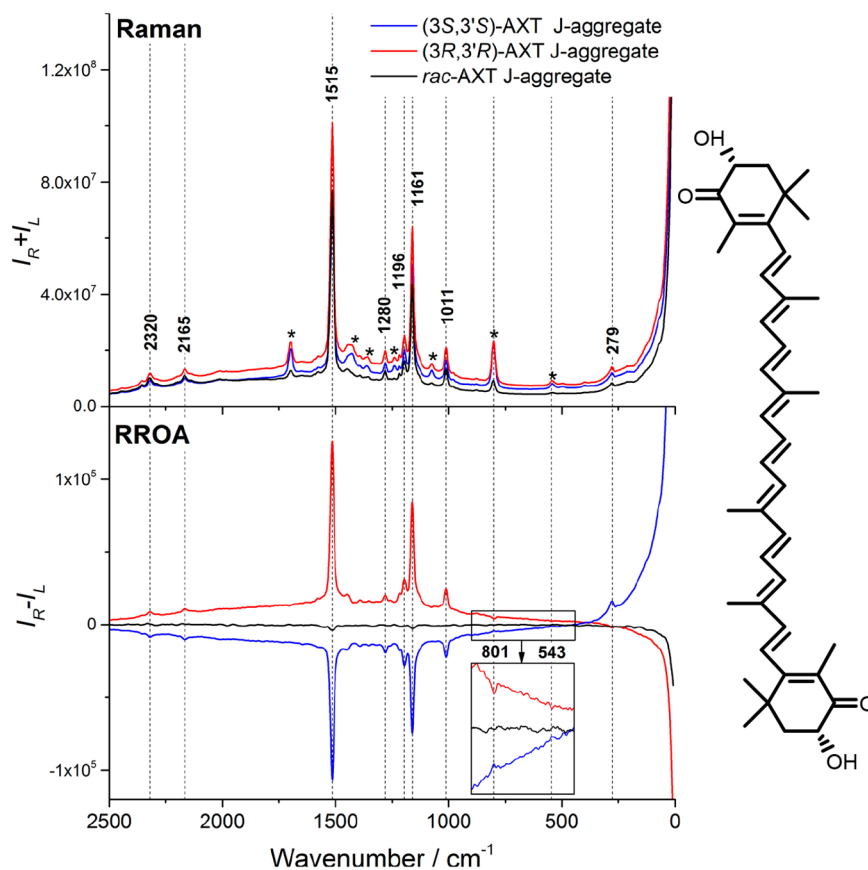


Figure 8. Raman and ROA of (3*R*,3'*R*)-astaxanthin (formula on the right), (3*S*,3'*S*)-astaxanthin, and racemic astaxanthin 3:7 water/acetone aggregates. Reprinted with permission from ref 4. Copyright 2016 ACS.

resonant with the laser radiation. Ideally, the aggregation is then monitored as a sudden rise/loss of ROA signal. Quite often, chiral supramolecular structures exhibit a strong ECD signal and, consequently, strong RROA.

AIRROA can also be thought of as a chirality amplification; for example, nonaggregated chiral xanthophylls alone provide very weak ROA.^{4,72–75} Xanthophylls, oxygenated carotenes, have a long polyene chain that is responsible for a strong electronic absorption within ~ 400 – 600 nm. UV–vis spectrum of xanthophylls and other carotenoids is dominated by the $S_0 \rightarrow S_2$ (in terms of local symmetry, $1^1A_g^- \rightarrow 1^1B_u^+$) transition, which is also responsible for the strong resonance and preresonance enhancements in the Raman scattering. Although xanthophylls are often chiral, the $S_0 \rightarrow S_2$ rotational strength is rather weak. The sources of chirality, stereogenic centers, are usually located at molecular termini, and do not much affect symmetry of the polyene chains. The situation is changed after aggregation, where the flat polyene chains in monomers are stacked next to each other in a chiral manner, in a supramolecular structure. Exciton splitting of the $S_0 \rightarrow S_2$ transitions and the chiral packing usually results in a strong ECD couplet and RROA signal.

First AIRROA spectra were reported for (3*R*,3'*R*)- and (3*S*,3'*S*)-astaxanthin “J-aggregates” suspended in water/acetone environment (Figure 8).⁴ Later, this phenomenon was confirmed for zeaxanthin, lutein, and lutein derivatives.^{74,75} The examples were measured on SCP-ROA BioTools spectrometer and 532 nm laser. Although the concentration ($\sim 1 \times 10^{-5}$ M) was unreasonably small for normal ROA spectroscopy, RROA spectra were quite strong. RROA of

astaxanthin aggregates were monosigned, opposite in sign to 532 nm ECD, and the (3*R*,3'*R*) and (3*S*,3'*S*) enantiomers provided “mirror image” spectra. RROA intensities were almost perfectly proportional to Raman, the main bands occurred at 1515 cm^{-1} (ν_1 , C=C stretching), 1161 and 1011 cm^{-1} (ν_2 , ν_3 , C–C stretchings). Also overtones ($2\nu_2$, 2320 cm^{-1}) and combination bands ($\nu_2 + \nu_3$, 2165 cm^{-1}) were visible.

The aggregation reminds one of the spectroscopic behavior of the OCP protein.⁵¹ After aggregation (J-astaxanthin aggregates), the ν_1 band shifted from 1520 to 1515 cm^{-1} , and the hydrogen out of plane band decreased in intensity. These spectral changes are related to the prolongation of the effective conjugation in the polyene chain, and a less distorted conformation in the aggregates. CIDs were measured as $\sim 1.4 \times 10^{-3}$ for (3*R*,3'*R*)-, and $\sim -1.5 \times 10^{-3}$ for (3*S*,3'*S*)-astaxanthin, exceptionally high values for the ROA spectroscopy. For combination bands and overtones, the CIDs were by about $\sim 50\%$ smaller. CIDs were not $-g/2$ as in the SES theory, but rather approached $-g$.⁴

Other carotenoids often behave differently. Zeaxanthin aggregates gave CIDs seven times smaller than g , and the RROA signal was dependent on the aggregate type.⁷⁴ Strongly coupled “H-aggregates” of astaxanthin, and lutein exhibited a huge hypsochromic shift of the $S_0 \rightarrow S_2$ transition (e.g., down to ~ 380 nm, farther from the excitation line), and RROA was not present.^{73,75}

The AIRROA effect was also detected for carotenoid microcrystals extracted from carrot root cells. The microcrystals consisted of $\sim 95\%$ achiral β -carotene and only small amounts of chiral α -carotene and lutein. Thus, the observed intense ECD

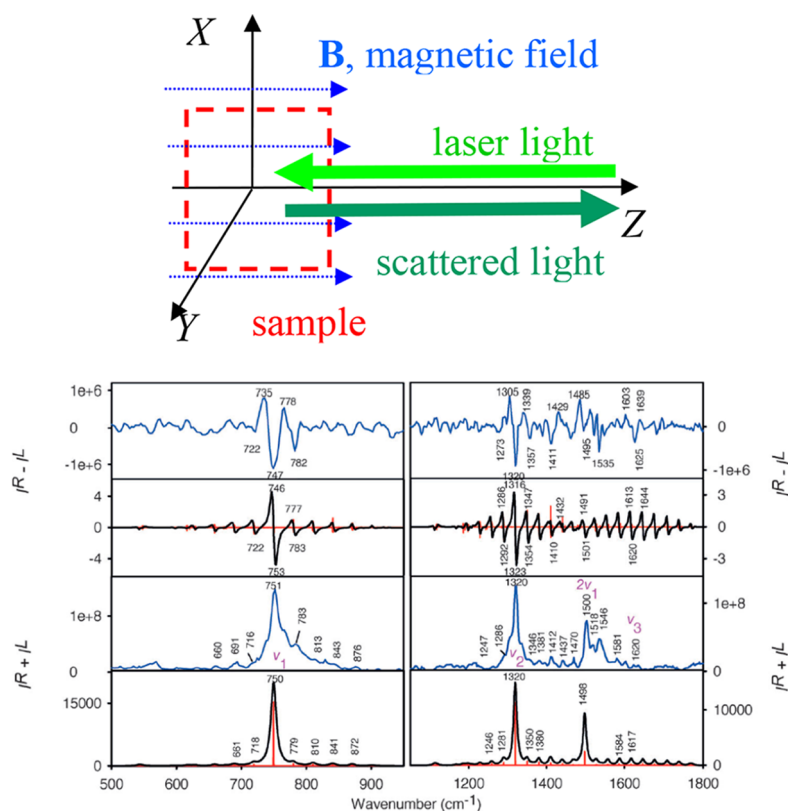


Figure 9. Geometry of the experiment (top), and experimental (blue) and simulated (black) magnetic RROA and Raman spectra of NO₂. Reprinted with permission from ref 6. Copyright 2014 John Wiley and Sons.

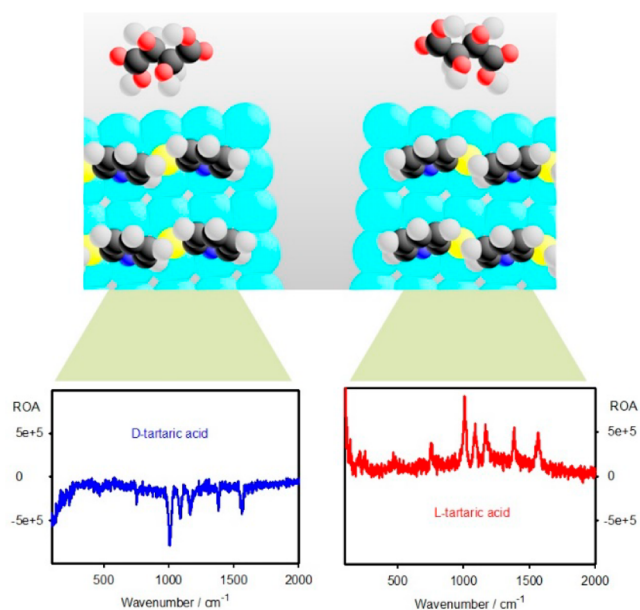


Figure 10. Scheme of the experiment when the chirality of “linker” molecules assembled on the silver surface (blue) is controlled by chiral molecules (top) in the solution. SEROA spectra of the linker are detected. Reprinted with permission from ref 97. Copyright 2021 RSC.

and RROA signals were explained by the “sergeants-and-soldiers” behavior. This was confirmed for a number of model aggregates. A small number of chiral molecules—sergeants—transfers the chirality to aggregated achiral building blocks—soldiers.⁷⁶

Gaseous Magnetic RROA. Measurement of natural ROA for gases is quite difficult, and so far the experiment was reported only for methyloxirane.⁷⁷ Also, ROA induced by the magnetic field is almost zero for nonabsorbing molecules.²⁶ In resonance, however, both modalities seem to be easily possible. Magnetic RROA of ferrocyanochrome *c* was recorded, for example, already in the 1980s.⁷⁸ In gases, magnetic RROA was observed for nitrogen dioxide, chlorine, bromine, and iodine.^{5,6}

The paramagnetic nitrogen dioxide was measured in a field of 1.5 T, with the 532 nm excitation. The signal was enhanced due to the resonance, but also because of the large molecular magnetic moment causing the Zeeman splitting of rotational levels in the magnetic field. The RROA spectrum had a surprising number of features, was bisignate, overtone transitions were visible, and it could be rationalized by simulations based on the Fermi golden rule and angular momentum theory (Figure 9). An interesting possibility to determine individual polarizability components from the spectra was suggested.⁶

Even more surprising was the fact that (only somewhat weaker) magnetic RROA could be measured also in diamagnetic halogen gases (Cl₂, Br₂, I₂). Their ground state magnetic moment is about 2000 times smaller than for NO₂ (cf. Bohr vs nuclear magneton), and associated splitting of the rotational levels is negligible. However, Raman scattering also involves excited electronic states that are paramagnetic, and simulations showed that they can thus support measurable signal.⁵

Surface-Enhanced (R)ROA, Measurements with Colloids. In theory, a combination of surface enhanced Raman scattering and ROA (“SEROA”) can provide extreme sensitivity. The excitation light is in a “plasmon” resonance with electronic states of the nanoparticles, and other enhancement mechanisms

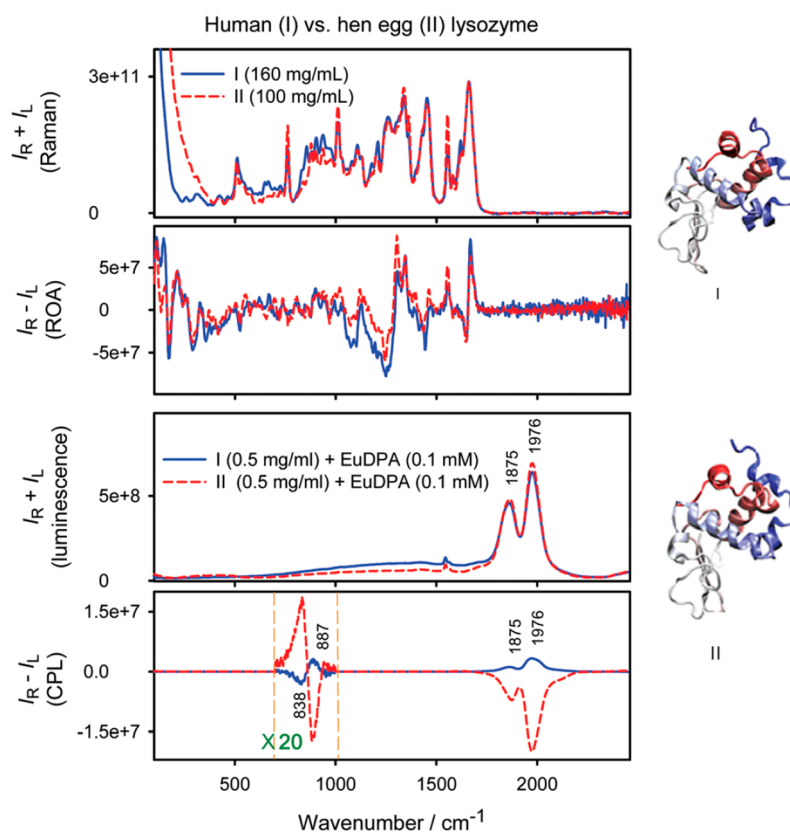


Figure 11. Raman and ROA spectra as well as luminescence and CPL of human milk and hen-egg lysozyme. Reprinted with permission from ref 103. Copyright 2016 Wiley.

can be present.⁹ First theoretical SEROA studies appeared in the 1980s by Efrima,^{79,80} a renewed interest came after a longer pause.^{81–89}

Early experimental studies were not convincing.⁹⁰ Met-enkephalin SEROA spectra were reported as measured on silver colloids, using a ChiralRaman SCP-ROA instrument and 532 nm excitation.⁹¹ About 100 times lower concentration, and 3 times shorter acquisition times were used compared to the usual ROA measurement, indicating thus the potential of the method. SEROA was also observed for myoglobin, cytochrome *c*, and hemoglobin.^{60,61,92,93} A typical trouble was the instability of the colloids, measurement artifacts, and time-dependent unstable ROA signal.

Later, “intelligent” colloids stabilized by a polymer,⁹⁴ silica shell,⁹⁵ or differently shaped metallic nanostructures⁹⁶ gave better results. For example, SEROA spectra of D- and L-ribose already exhibited reasonable mirror-image symmetry.⁹⁴ The silver colloid was stabilized by poly(acrylic acid). In another experiment, achiral dye, “reporter”, was attached to the silver nanoparticle stabilized by a silica shell.⁹⁵ The benzotriazole dye had an absorption maximum at 514 nm, close to the 532 nm excitation line. It provided SEROA; i.e., it became chiral in the presence of chiral molecules in the environment, although the reproducibility was limited.

Similarly as for AIRROA, also for SEROA the sergeants-and-soldiers principle was applied, when chiral acids (e.g., tartaric) imposed their chirality on achiral aromatic linkers (such as 2-mercaptopyridine) attached to the silver nanoparticle surface.⁹⁷ The reliability was verified with enantiomers for several chiral compounds (Figure 10). The SEROA thus needs to be further

developed, but it is already starting to show the potential for detection of molecules at low concentrations.

Circularly Polarized Luminescence (CPL) Measured on ROA Spectrometers.

Luminescence is, of course, a different physical phenomenon than ROA. We mention it here because CPL can be conveniently measured on ROA spectrometers,⁹⁸ it exhibits some properties of RROA, and sometimes it is difficult to experimentally distinguish these two spectral kinds.⁹⁹ For example, CPL was incorrectly interpreted as induced resonance ROA (IRROA).¹⁰⁰ Unlike for ROA/RROA, relative positions of CPL bands with respect to the excitation frequency are dependent on the excitation wavelength, and the degree of circularity is zero.⁹⁸ For the commercial BioTools SCP-ROA spectrometer we are limited to 532–614 nm range (~ 0 –2500 cm^{-1} Raman shift), and a luminescence of organic compounds with broad bands is rather a harbinger of problems. However, CPL of lanthanide ions measured in this way, in particular that of Eu(III) that exhibits many narrow bands even in this region, seems to be quite useful. Lanthanide electronic transitions are often nearly forbidden,¹⁰¹ and their detection can profit from the ROA technology.^{102,103}

The lanthanide luminescence is also very sensitive to the environment, and changed/induced chirality of lanthanide ions and complexes can be used to study various biomolecules. The CPL/ROA method has been used to probe sugars,¹⁰³ proteins,¹⁰² peptides,¹⁰⁴ and nucleic acids.^{105,106} The chirality is often induced via perturbed equilibrium of the Δ and Λ forms of complexes, symmetry of which is close to D_3 . An example of such experiments is in Figure 11, where CPL of the $[\text{Eu}(\text{DPA})_3]^{3-}$ ion was substantially different in the presence

of very similar proteins, human and chicken lysozymes, even though their Raman and ROA spectra were virtually indistinguishable.¹⁰³

CONCLUSIONS

We were trying to provide examples and opinions on the whereabouts of the resonance Raman optical activity, which seems to be developing to a rich and interesting field of chiral spectroscopy. It spans rotational spectroscopy of gases as well as biomolecular studies, such as those of functional proteins. In the future, it may become even more important as more flexible spectrometers are available, such as those operating at the UV region, or with variable excitation wavelengths.

Natural molecular vibrational RROA is a unique molecular property that bears information about molecular geometry and structure of the electronic cloud. Compared to a far from resonance ROA, the spectra are stronger, can be detected in lower sample amounts, and may sample molecules more locally, in the vicinity of the chromophore. RROA may be accompanied by partially related (ECD, polarized Raman) or quite unrelated (CPLu) phenomena.

RROA measurements thus still comprise many dangers, such as sample decomposition, signal mixing with the ECD-Raman effect, and experiment misinterpretations. Better theoretical tools for spectra simulations are needed as well.

AUTHOR INFORMATION

Corresponding Authors

Grzegorz Zajac – Jagiellonian Centre for Experimental Therapeutics (JCET), Jagiellonian University, Krakow 30-348, Poland; orcid.org/0000-0003-4090-9334; Email: grzesiek.zajac@uj.edu.pl

Petr Bouř – Institute of Organic Chemistry and Biochemistry, Academy of Sciences, Prague 16610, Czech Republic; orcid.org/0000-0001-8469-1686; Email: bouř@uochb.cas.cz

Complete contact information is available at:
<https://pubs.acs.org/10.1021/acs.jpcb.1c08370>

Notes

The authors declare no competing financial interest.

Biographies



Grzegorz Zajac received a M.Sc. degree in chemistry in 2014 and a Ph.D. degree in 2018, both from the Faculty of Chemistry, Jagiellonian University in Krakow, under the guidance of Prof. Malgorzata Baranska. During his postdoctoral work he also stayed at the Institute of Organic Chemistry and Biochemistry, Prague. Currently he is a researcher in the

Jagiellonian Centre for Experimental Therapeutics (JCET), Jagiellonian University in Krakow. His research focuses on computational and spectroscopic studies of biomolecular systems, especially by means of chiroptical methods.



Petr Bouř obtained his master's degree in physics at the Charles University, Prague, and CSc. (PhD. equivalent) degree in organic chemistry in 1993 at the Czechoslovak Academy of Sciences, Prague, in a joint program with the University of Illinois at Chicago. From 2007 he has been a leader of the Molecular Spectroscopy group in the Institute of Organic Chemistry and Biochemistry and at 2013 he became a full professor at the University of Chemistry and Technology, Prague. His research interest comprises development of molecular dynamics and quantum chemical computational procedures for spectroscopy and experimental and theoretical aspects of vibrational optical activity.

ACKNOWLEDGMENTS

This work was funded by the National Science Centre Poland (2019/35/B/ST4/04161) and the Ministry of Education (CZ.02.1.01/0.0/0.0/16019/0000729) and Science Foundation (20-10144S) of the Czech Republic.

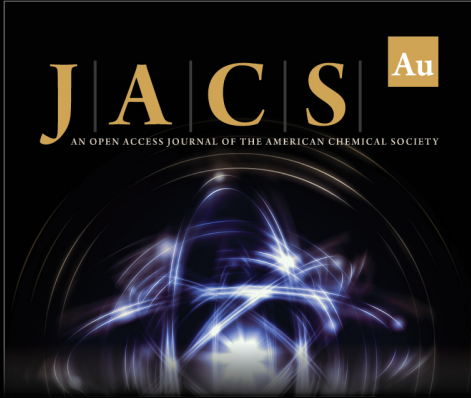
REFERENCES

- (1) Berg, R. W.; Shim, I.; White, P. C.; Abdali, S. Raman Optical Activity and Raman Spectra of Amphetamine Species-Quantum Chemical Model Calculations and Experiments. *Am. J. Anal. Chem.* **2012**, *03*, 410–421.
- (2) Vargek, M.; Freedman, T. B.; Lee, E.; Nafie, L. A. Experimental Observation of Resonance Raman Optical Activity. *Chem. Phys. Lett.* **1998**, *287*, 359–364.
- (3) Machalska, E.; Zajac, G.; Gruca, A.; Zobi, F.; Baranska, M.; Kaczor, A. Resonance Raman Optical Activity Shows Unusual Structural Sensitivity for Systems in Resonance with Multiple Excited States: Vitamin B₁₂ Case. *J. Phys. Chem. Lett.* **2020**, *11*, S037–S043.
- (4) Zajac, G.; Kaczor, A.; Pallares Zazo, A.; Mlynarski, J.; Dudek, M.; Baranska, M. Aggregation-Induced Resonance Raman Optical Activity (AIRROA): A New Mechanism for Chirality Enhancement. *J. Phys. Chem. B* **2016**, *120*, 4028–4033.
- (5) Šebestík, J.; Kapitán, J.; Pačes, O.; Bouř, P. Diamagnetic Raman Optical Activity of Chlorine, Bromine, and Iodine Gases. *Angew. Chem., Int. Ed.* **2016**, *55*, 3504–3508.
- (6) Šebestík, J.; Bouř, P. Observation of Paramagnetic Raman Optical Activity of Nitrogen Dioxide. *Angew. Chem., Int. Ed.* **2014**, *53*, 9236–9239.
- (7) Wu, T.; Li, G.; Kapitán, J.; Kessler, J.; Xu, Y.; Bouř, P. Two Spectroscopies in One: Interference of Circular Dichroism and Raman Optical Activity. *Angew. Chem., Int. Ed.* **2020**, *59*, 21895–21898.
- (8) Machalska, E.; Zajac, G.; Wierzba, A. J.; Kapitán, J.; Andruniów, T.; Spiegel, M.; Gryko, D.; Bouř, P.; Baranska, M. Recognition of the True and False Resonance Raman Optical Activity. *Angew. Chem., Int. Ed.* **2021**, *60*, 21205–21210.

- (9) Jensen, L.; Autschbach, J.; Krykunov, M.; Schatz, G. C. Resonance Vibrational Raman Optical Activity: A Time-Dependent Density Functional Theory Approach. *J. Chem. Phys.* **2007**, *127*, 134101.
- (10) Nafie, L. A. Theory of Resonance Raman Optical Activity: The Single Electronic State Limit. *Chem. Phys.* **1996**, *205*, 309–322.
- (11) Baiardi, A.; Bloino, J.; Barone, V. Time-Dependent Formulation of Resonance Raman Optical Activity Spectroscopy. *J. Chem. Theory Comput.* **2018**, *14*, 6370–6390.
- (12) Mattiat, J.; Luber, S. Vibrational (Resonance) Raman Optical Activity with Real Time Time Dependent Density Functional Theory. *J. Chem. Phys.* **2019**, *151*, 234110.
- (13) Barron, L. D.; Bogaard, M. P.; Buckingham, A. D. Raman Scattering of Circularly Polarized Light by Optically Active Molecules. *J. Am. Chem. Soc.* **1973**, *95*, 603–605.
- (14) Keiderling, T. A. Structure of Condensed Phase Peptides: Insights from Vibrational Circular Dichroism and Raman Optical Activity Techniques. *Chem. Rev.* **2020**, *120*, 3381–3419.
- (15) Costante, J.; Hecht, L.; Polavarapu, P. L.; Collet, A.; Barron, L. D. Absolute Configuration of Bromochlorofluoromethane from Experimental and Ab Initio Theoretical Vibrational Raman Optical Activity. *Angew. Chem., Int. Ed.* **1997**, *36*, 885–887.
- (16) Haesler, J.; Schindelholz, I.; Riguet, E.; Bochet, C. G.; Hug, W. Absolute Configuration of Chirally Deuterated Neopentane. *Nature* **2007**, *446*, 526–529.
- (17) Dudek, M.; Zajac, G.; Szafraniec, E.; Wiercigroch, E.; Tott, S.; Malek, K.; Kaczor, A.; Baranska, M. Raman Optical Activity and Raman Spectroscopy of Carbohydrates in Solution. *Spectrochim. Acta, Part A* **2019**, *206*, 597–612.
- (18) Palivec, V.; Michal, P.; Kapitán, J.; Martínez-Seara, H.; Bouř, P. Raman Optical Activity of Glucose and Sorbose in Extended Wavenumber Range. *ChemPhysChem* **2020**, *21*, 1272–1279.
- (19) Blanch, E. W.; Hecht, L.; Barron, L. D. Vibrational Raman Optical Activity of Proteins, Nucleic Acids, and Viruses. *Methods* **2003**, *29*, 196–209.
- (20) Barron, L. D.; Blanch, E. W.; McColl, I. H.; Syme, C. D.; Hecht, L.; Nielsen, K. Structure and Behaviour of Proteins, Nucleic Acids and Viruses from Vibrational Raman Optical Activity. *Spectroscopy* **2003**, *17*, 101–126.
- (21) Jacob, C. R.; Luber, S.; Reiher, M. Calculated Raman Optical Activity Signatures of Tryptophan Side Chains. *ChemPhysChem* **2008**, *9*, 2177–2180.
- (22) Yamamoto, S.; Straka, M.; Watarai, H.; Bouř, P. Formation and Structure of the Potassium Complex of Valinomycin in Solution Studied by Raman Optical Activity Spectroscopy. *Phys. Chem. Chem. Phys.* **2010**, *12*, 11021–11032.
- (23) Pančoška, P.; Barron, L. D.; Krimm, S.; Keiderling, T. A.; Nafie, L. A.; Diem, M.; Polavarapu, P. L.; Ford, S. J.; Woody, R. W. General Discussion. *Faraday Discuss.* **1994**, *99*, 311–326.
- (24) Weymuth, T.; Reiher, M. Characteristic Raman Optical Activity Signatures of Protein β -Sheets. *J. Phys. Chem. B* **2013**, *117*, 11943–11953.
- (25) Luber, S.; Reiher, M. Theoretical Raman Optical Activity Study of the β Domain of Rat Metallothionein. *J. Phys. Chem. B* **2010**, *114*, 1057–1063.
- (26) Barron, L. D. *Molecular Light Scattering and Optical Activity*; Cambridge University Press: Cambridge, U.K., 2004.
- (27) Hug, W. Virtual Enantiomers as the Solution of Optical Activity's Deterministic Offset Problem. *Appl. Spectrosc.* **2003**, *57*, 1–13.
- (28) Hug, W.; Hangartner, G. A Novel High-Throughput Raman Spectrometer for Polarization Difference Measurements. *J. Raman Spectrosc.* **1999**, *30*, 841–852.
- (29) Kapitán, J.; Barron, L. D.; Hecht, L. A Novel Raman Optical Activity Instrument Operating in the Deep Ultraviolet Spectral Region. *J. Raman Spectrosc.* **2015**, *46*, 392–399.
- (30) Asher, S. A.; Ianoul, A.; Mix, G.; Boyden, M. N.; Karnoup, A.; Diem, M.; Schweitzer-Stenner, R. Dihedral Psi Angle Dependence of the Amide III Vibration: A Uniquely Sensitive UV Resonance Raman Secondary Structural Probe. *J. Am. Chem. Soc.* **2001**, *123*, 11775–11781.
- (31) Asher, S. A. Ultraviolet Raman Spectrometry. In *Handbook of Vibrational Spectroscopy*; Chalmers, J. M., Griffiths, P. R., Eds.; John Wiley & Sons Ltd.: Chichester, U.K., 2002.
- (32) Nafie, L. *Vibrational Optical Activity: Principles and Applications*; Wiley: Chichester, U.K., 2011.
- (33) Angeli, C.; Bak, K. L.; Bakken, V.; Christiansen, O.; Cimiriaglia, R.; Coriani, S.; Dahle, P.; Dalskov, E. K.; Enevoldsen, T.; Fernandez, B.; et al. *Dalton 2011, a Molecular Electronic Structure Program*; Release 2.0 ed.; University of Oslo: Oslo, 2005–2009.
- (34) Frisch, M. J.; Trucks, G. W.; Schlegel, H. B.; Scuseria, G. E.; Robb, M. A.; Cheeseman, J. R.; Scalmani, G.; Barone, V.; Petersson, G. A.; Nakatsuji, H.; et al. *Gaussian 16*, Rev. A.03; Gaussian, Inc.: Wallingford, CT, 2016.
- (35) Klamt, A. Turbomole. In *The Encyclopedia of Computational Chemistry*; Schleyer, P. R., Allinger, N. L., Clark, T., Gasteiger, J., Kollman, P. A., Schaefer, H. F., III, Schreiner, P. R., Eds.; John Wiley & Sons: Chichester, U.K., 1998; Vol. 3; pp 604–615.
- (36) Baerends, E. J.; Ziegler, T.; Autschbach, J.; Bashford, D.; Bérces, A.; Bickelhaupt, F. M.; Bo, C.; Boerrigter, P. M.; Cavallo, L.; Chong, D. P.; et al. *ADF2013*; SCM, Theoretical Chemistry, Vrije Universiteit: Amsterdam, The Netherlands, 2013.
- (37) Helgaker, T.; Ruud, K.; Bak, K. L.; Joergensen, P.; Olsen, J. Vibrational Raman Optical Activity Calculations Using London Atomic Orbitals. *Faraday Discuss.* **1994**, *99*, 165–180.
- (38) Liegeois, V.; Ruud, K.; Champagne, B. An Analytical Derivative Procedure for the Calculation of Vibrational Raman Optical Activity Spectra. *J. Chem. Phys.* **2007**, *127*, 204105.
- (39) Ruud, K.; Helgaker, T.; Bouř, P. Gauge-Origin Independent Density-Functional Theory Calculations of Vibrational Raman Optical Activity. *J. Phys. Chem. A* **2002**, *106*, 7448–7455.
- (40) Cheeseman, J. R.; Frisch, M. J. Basis Set Dependence of Vibrational Raman and Raman Optical Activity Intensities. *J. Chem. Theory Comput.* **2011**, *7*, 3323–3334.
- (41) Helgaker, T.; Coriani, S.; Jorgensen, P.; Kristensen, K.; Olsen, J.; Ruud, K. Recent Advances in Wave Function-Based Methods of Molecular-Property Calculations. *Chem. Rev.* **2012**, *112*, 543–631.
- (42) Vidal, L. N.; Egidij, F.; Barone, V.; Cappelli, C. Origin Invariance in Vibrational Resonance Raman Optical Activity. *J. Chem. Phys.* **2015**, *142*, 174101.
- (43) Li, G.; Alshalalfeh, M.; Yang, W.; Cheeseman, J. R.; Bouř, P.; Xu, Y. Can One Measure Resonance Raman Optical Activity? *Angew. Chem., Int. Ed.* **2021**, *60*, 22004–22009.
- (44) Nafie, L. A.; Brinson, B. E.; Cao, X.; Rice, D. A.; Rahim, O. M.; Dukor, R. K.; Halas, N. J. Near-Infrared Excited Raman Optical Activity. *Appl. Spectrosc.* **2007**, *61*, 1103–1106.
- (45) Unno, M.; Kikukawa, T.; Kumauchi, M.; Kamo, N. Exploring the Active Site Structure of a Photoreceptor Protein by Raman Optical Activity. *J. Phys. Chem. B* **2013**, *117*, 1321–1325.
- (46) Zhang, Y.; Wang, P.; Jia, G.; Cheng, F.; Feng, Z.; Li, C. A Short-Wavelength Raman Optical Activity Spectrometer with Laser Source at 457nm for the Characterization of Chiral Molecules. *Appl. Spectrosc.* **2017**, *71*, 2211–2217.
- (47) Šugar, J.; Bouř, P. Quantitative Analysis of Sugar Composition in Honey Using 532 nm Excitation Raman and Raman Optical Activity Spectra. *J. Raman Spectrosc.* **2016**, *47*, 1298–1303.
- (48) Polavarapu, P. L. Fourier Transform Raman Optical Activity. *Chem. Phys. Lett.* **1988**, *148*, 21–25.
- (49) Krupová, M.; Kessler, J.; Bouř, P. Recent Trends in Chiroptical Spectroscopy: Theory and Applications of Vibrational Circular Dichroism and Raman Optical Activity. *ChemPlusChem* **2020**, *85*, 561–575.
- (50) Haraguchi, S.; Hara, M.; Shingae, T.; Kumauchi, M.; Hoff, W. D.; Unno, M. Experimental Detection of the Intrinsic Difference in Raman Optical Activity of a Photoreceptor Protein under Preresonance and Resonance Conditions. *Angew. Chem., Int. Ed.* **2015**, *54*, 11555–11558.
- (51) Fujisawa, T.; Leverenz, R. L.; Nagamine, M.; Kerfeld, C. A.; Unno, M. Raman Optical Activity Reveals Carotenoid Photoactivation


- Events in the Orange Carotenoid Protein in Solution. *J. Am. Chem. Soc.* **2017**, *139*, 10456–10460.
- (52) Ianoul, A.; Mikhonin, A.; Lednev, I. K.; Asher, S. A. UV Resonance Raman Study of the Spatial Dependence of α -Helix Unfolding. *J. Phys. Chem. A* **2002**, *106*, 3621–3624.
- (53) Li, G.; Kessler, J.; Cheramy, J.; Wu, T.; Poopari, M. R.; Bouř, P.; Xu, Y. Transfer and Amplification of Chirality within the 'Ring of Fire' Observed in Resonance Raman Optical Activity Experiments. *Angew. Chem., Int. Ed.* **2019**, *58*, 16495–16498.
- (54) Šebestík, J.; Teplý, F.; Čisářová, I.; Vávra, J.; Koval, D.; Bouř, P. Intense Chirality Induction in Nitrile Solvents by a Helquat Dye Monitored by near Resonance Raman Scattering. *Chem. Commun.* **2016**, *52*, 6257–6260.
- (55) Machalska, E.; Zajac, G.; Baranska, M.; Kaczorek, D.; Kawęcki, R.; Lipiński, P. F. J.; Rode, J. E.; Dobrowolski, J. C. On Raman Optical Activity Sign-Switching between the Ground and Excited States Leading to an Unusual Resonance ROA Induced Chirality. *Chem. Sci.* **2021**, *12*, 911–916.
- (56) Hecht, L.; Barron, L. D. Instrument for Natural and Magnetic Raman Optical Activity Studies in Right-Angle Scattering. *J. Raman Spectrosc.* **1994**, *25*, 443–451.
- (57) Machalska, E.; Hachlica, N.; Zajac, G.; Carraro, D.; Baranska, M.; Licini, G.; Bouř, P.; Zonta, C.; Kaczor, A. Chiral Recognition Via a Stereodynamic Vanadium Probe Using ECD-ROA Interference. *Phys. Chem. Chem. Phys.* **2021**, *23*, 23336–23340.
- (58) Lubner, S.; Neugebauer, J.; Reiher, M. Enhancement and De-Enhancement Effects in Vibrational Resonance Raman Optical Activity. *J. Chem. Phys.* **2010**, *132*, 044113.
- (59) Krausbeck, F.; Autschbach, J.; Reiher, M. Calculated Resonance Vibrational Raman Optical Activity Spectra of Naproxen and Ibuprofen. *J. Phys. Chem. A* **2016**, *120*, 9740–9748.
- (60) Abdali, S.; Johannessen, C.; Nygaard, J.; Nørbygaard, T. Resonance Surface Enhanced Raman Optical Activity of Myoglobin as a Result of Optimized Resonance Surface Enhanced Raman Scattering Conditions. *J. Phys.: Condens. Matter* **2007**, *19*, 285205.
- (61) Johannessen, C.; White, P. C.; Abdali, S. Resonance Raman Optical Activity and Surface Enhanced Resonance Raman Optical Activity Analysis of Cytochrome C. *J. Phys. Chem. A* **2007**, *111*, 7771–7776.
- (62) Hopmann, K. H.; Šebestík, J.; Novotná, J.; Stensen, W.; Urbanová, M.; Svenson, J.; Svendsen, J. S.; Bouř, P.; Ruud, K. Determining the Absolute Configuration of Two Marine Compounds Using Vibrational Chiroptical Spectroscopy. *J. Org. Chem.* **2012**, *77*, 858–869.
- (63) Merten, C.; Li, H.; Nafie, L. A. Simultaneous Resonance Raman Optical Activity Involving Two Electronic States. *J. Phys. Chem. A* **2012**, *116*, 7329–7336.
- (64) Magg, M.; Kadria-Vili, Y.; Oulevey, P.; Weisman, R. B.; Bürgi, T. Resonance Raman Optical Activity Spectra of Single-Walled Carbon Nanotube Enantiomers. *J. Phys. Chem. Lett.* **2016**, *7*, 221–225.
- (65) Nagy, P. R.; Biró, L.; Koltai, J.; Surján, P. R.; Szabados, Á.; Kürti, J. Theoretical Vibrational Optical Activity of Chiral Carbon Nanoparticles: Fullerenes and Carbon Nanotubes. *Phys. Status Solidi B* **2014**, *251*, 2451–2456.
- (66) Nagy, P. R.; Koltai, J.; Surján, P. R.; Kürti, J.; Szabados, Á. Resonance Raman Optical Activity of Single Walled Chiral Carbon Nanotubes. *J. Phys. Chem. A* **2016**, *120*, 5527–5538.
- (67) Shen, C.; Loas, G.; Srebro-Hooper, M.; Vanthuyne, N.; Toupet, L.; Cador, O.; Paul, F.; López Navarrete, J. T.; Ramírez, F. J.; Nieto-Ortega, B.; et al. Iron Alkynyl Helicenes: Redox-Trigged Chiroptical Tuning in the IR and near-IR Spectral Regions and Suitable for Telecommunications Applications. *Angew. Chem., Int. Ed.* **2016**, *55*, 8062–8066.
- (68) Shen, C.; Srebro-Hooper, M.; Weymuth, T.; Krausbeck, F.; Navarrete, J. T. L.; Ramírez, F. J.; Nieto-Ortega, B.; Casado, J.; Reiher, M.; Autschbach, J.; et al. Redox-Active Chiroptical Switching in Mono- and Bis-Iron Ethynylcarbo[6]Helicenes Studied by Electronic and Vibrational Circular Dichroism and Resonance Raman Optical Activity. *Chem. - Eur. J.* **2018**, *24*, 15067–15079.
- (69) Sgammato, R.; Herrebout, W.; Johannessen, C. Resonance Raman Optical Activity of the Imidazole–Myoglobin Complex: Titrating Enhancement. *J. Raman Spectrosc.* **2019**, *50*, 1905–1913.
- (70) Bogaerts, J.; Johannessen, C. On/Off Resonance Raman Optical Activity of Human Serum Transferrin. *J. Raman Spectrosc.* **2019**, *50*, 641–646.
- (71) Machalska, E.; Zajac, G.; Halat, M.; Wierzba, A. J.; Gryko, D.; Baranska, M. Resonance Raman Optical Activity Spectroscopy in Probing Structural Changes Invisible to Circular Dichroism Spectroscopy: A Study on Truncated Vitamin B₁₂ Derivatives. *Molecules* **2020**, *25*, 4386.
- (72) Zajac, G.; Kaczor, A.; Buda, S.; Młynarski, J.; Frelek, J.; Dobrowolski, J.; Baranska, M. Prediction of ROA and ECD Related to Conformational Changes of Astaxanthin Enantiomers. *J. Phys. Chem. B* **2015**, *119*, 12193–12201.
- (73) Dudek, M.; Zajac, G.; Kaczor, A.; Baranska, M. Aggregation-Induced Resonance Raman Optical Activity (AIRROA) and Time-Dependent Helicity Switching of Astaxanthin Supramolecular Assemblies. *J. Phys. Chem. B* **2016**, *120*, 7807–7814.
- (74) Dudek, M.; Zajac, G.; Kaczor, A.; Baranska, M. Resonance Raman Optical Activity of Zeaxanthin Aggregates. *J. Raman Spectrosc.* **2017**, *48*, 673–679.
- (75) Zajac, G.; Lasota, J.; Dudek, M.; Kaczor, A.; Baranska, M. Pre-Resonance Enhancement of Exceptional Intensity in Aggregation-Induced Raman Optical Activity (AIROA) Spectra of Lutein Derivatives. *Spectrochim. Acta, Part A* **2017**, *173*, 356–360.
- (76) Dudek, M.; Machalska, E.; Oleszkiewicz, T.; Grzebelus, E.; Baranski, R.; Szcześniak, P.; Młynarski, J.; Zajac, G.; Kaczor, A.; Baranska, M. Chiral Amplification in Nature: Studying Cell-Extracted Chiral Carotenoid Microcrystals Via the Resonance Raman Optical Activity of Model Systems. *Angew. Chem., Int. Ed.* **2019**, *58*, 8383–8388.
- (77) Šebestík, J.; Bouř, P. Raman Optical Activity of Methyloxirane Gas and Liquid. *J. Phys. Chem. Lett.* **2011**, *2*, 498–502.
- (78) Barron, L. D.; Meehan, C.; Vrbancich, J. Magnetic Resonance-Raman Optical Activity of Ferrocytochrome C Theory and Experiment. *J. Raman Spectrosc.* **1982**, *12*, 251–261.
- (79) Efrima, S. The Effect of Large Electric Field Gradients on the Raman Optical Activity of Molecules Adsorbed on Metal Surfaces. *Chem. Phys. Lett.* **1983**, *102*, 79–82.
- (80) Efrima, S. Raman Optical Activity of Molecules Adsorbed on Metal Surfaces: Theory. *J. Chem. Phys.* **1985**, *83*, 1356–1362.
- (81) Janesko, B. G.; Scuseria, G. E. Surface Enhanced Raman Optical Activity of Molecules on Orientationally Averaged Substrates: Theory of Electromagnetic Effects. *J. Chem. Phys.* **2006**, *125*, 124704.
- (82) Janesko, B. G.; Scuseria, G. E. Molecule-Surface Orientational Averaging in Surface Enhanced Raman Optical Activity Spectroscopy. *J. Phys. Chem. C* **2009**, *113*, 9445–9449.
- (83) Lombardini, R.; Acevedo, R.; Halas, N. J.; Johnson, B. R. Plasmonic Enhancement of Raman Optical Activity in Molecules near Metal Nanoshells: Theoretical Comparison of Circular Polarization Methods. *J. Phys. Chem. C* **2010**, *114*, 7390–7400.
- (84) Bouř, P. Matrix Formulation of the Surface-Enhanced Raman Optical Activity. *J. Chem. Phys.* **2007**, *126*, 136101.
- (85) Novák, V.; Šebestík, J.; Bouř, P. Theoretical Modeling of the Surface-Enhanced Raman Optical Activity. *J. Chem. Theory Comput.* **2012**, *8*, 1714–1720.
- (86) Jensen, L. Surface-Enhanced Vibrational Raman Optical Activity: A Time-Dependent Density Functional Theory Approach. *J. Phys. Chem. A* **2009**, *113*, 4437–4444.
- (87) Chulhai, D. V.; Jensen, L. Simulating Surface-Enhanced Raman Optical Activity Using Atomistic Electrostatics-Quantum Mechanical Models. *J. Phys. Chem. A* **2014**, *118*, 9069–9079.
- (88) Wu, T.; Zhang, X.; Wang, R.; Zhang, X. D. Strongly Enhanced Raman Optical Activity in Molecules by Magnetic Response of Nanoparticles. *J. Phys. Chem. C* **2016**, *120*, 14795–14804.
- (89) Hu, L.; Xi, F.; Qy, L.; Fang, Y. Searching the Theoretical Ultimate Limits of Probing Surface-Enhanced Raman Optical Activity. *ACS Omega* **2018**, *3*, 1170–1177.


- (90) Abdali, S.; Blanch, E. W. Surface Enhanced Raman Optical Activity (SEROA). *Chem. Soc. Rev.* **2008**, *37*, 980–992.
- (91) Abdali, S. Observation of SERS Effect in Raman Optical Activity, a New Tool for Chiral Vibrational Spectroscopy. *J. Raman Spectrosc.* **2006**, *37*, 1341–1345.
- (92) Johannessen, C.; Abdali, S. Surface Enhanced Raman Optical Activity as an Ultra Sensitive Tool for Ligand Binding Analysis. *Spectroscopy* **2007**, *21*, 143.
- (93) Brazhe, N. A.; Brazhe, A. R.; Sosnovtseva, O. V.; Abdali, S. Novel Chiroptical Analysis of Hemoglobin by Surface Enhanced Resonance Raman Optical Activity Spectroscopy. *Chirality* **2009**, *21*, E307–E312.
- (94) Pour, S. O.; Bell, S. E. J.; Blanch, E. W. Use of a Hydrogel Polymer for Reproducible Surface Enhanced Raman Optical Activity (SEROA). *Chem. Commun.* **2011**, *47*, 4754–4756.
- (95) Ostovar pour, S. O.; Rocks, L.; Faulds, K.; Graham, D.; Parchaňský, V.; Bouř, P.; Blanch, E. W. Through-Space Transfer of Chiral Information Mediated by a Plasmonic Nanomaterial. *Nat. Chem.* **2015**, *7*, 591–596.
- (96) Sun, M.; Zhang, Z.; Wang, P.; Li, Q.; Ma, F.; Xu, H. Remotely Excited Raman Optical Activity Using Chiral Plasmon Propagation in Ag Nanowires. *Light: Sci. Appl.* **2013**, *2*, e112–e112.
- (97) Das, M.; Gangopadhyay, D.; Sebestík, J.; Habartová, L.; Michal, P.; Kapitán, J.; Bouř, P. Chiral Detection by Induced Surface-Enhanced Raman Optical Activity. *Chem. Commun.* **2021**, *57*, 6388–6391.
- (98) Wu, T.; Kapitán, J.; Mašek, V.; Bouř, P. Detection of Circularly Polarized Luminescence of a Cs-Eu^{III} Complex in Raman Optical Activity Experiments. *Angew. Chem., Int. Ed.* **2015**, *54*, 14933–14936.
- (99) Wu, T.; Kapitán, J.; Andrushchenko, V.; Bouř, P. Identification of Lanthanide(III) Luminophores in Magnetic Circularly Polarized Luminescence Using Raman Optical Activity Instrumentation. *Anal. Chem.* **2017**, *89*, 5043–5049.
- (100) Yamamoto, S.; Bouř, P. Detection of Molecular Chirality by Induced Resonance Raman Optical Activity in Europium Complexes. *Angew. Chem., Int. Ed.* **2012**, *51*, 11058–11061.
- (101) Binnemans, K. Interpretation of Europium(III) Spectra. *Coord. Chem. Rev.* **2015**, *295*, 1–45.
- (102) Wu, T.; Průša, J.; Kessler, J.; Dračinský, M.; Valenta, J.; Bouř, P. Detection of Sugars Via Chirality Induced in Europium(III) Compounds. *Anal. Chem.* **2016**, *88*, 8878–8885.
- (103) Wu, T.; Kessler, J.; Bouř, P. Chiral Sensing of Amino Acids and Proteins Chelating with Eu^{III} Complexes by Raman Optical Activity Spectroscopy. *Phys. Chem. Chem. Phys.* **2016**, *18*, 23803–23811.
- (104) Brichtová, E.; Hudecová, H.; Vřšková, N.; Sebestík, J.; Bouř, P.; Wu, T. Binding of Lanthanide Complexes to Histidine-Containing Peptides Probed by Raman Optical Activity Spectroscopy. *Chem. - Eur. J.* **2018**, *24*, 8664–8669.
- (105) Wu, T.; Bouř, P.; Andrushchenko, V. Europium (III) as a Circularly Polarized Luminescence Probe of DNA Structure. *Sci. Rep.* **2019**, *9*, 1068.
- (106) Sahoo, J.; Wu, T.; Klepetářová, B.; Valenta, J.; Bouř, P. Binuclear Lanthanide(III) Complexes with Chiral Ligands: Dynamic Equilibria in Solution and Binding with Nucleotides Studied by Spectroscopic Methods. *ChemPlusChem* **2020**, *85*, 694–700.



JACS Au
AN OPEN ACCESS JOURNAL OF THE AMERICAN CHEMICAL SOCIETY

Editor-in-Chief
Prof. Christopher W. Jones
Georgia Institute of Technology, USA

Open for Submissions 

pubs.acs.org/jacsau  ACS Publications
Most Trusted. Most Cited. Most Read.